Correlation Between Topography and Magnetic Surface Anisotropy in Epitaxial Fe Films on Vicinal-to-(001) Au Surfaces with Different Step Orientation

M. Rickart – INESC Microsistemas e Nanotecnologia

T. Mewes – Ohio State University

S. O. Demokritov and B. Hillebrands – University of Kaiserslautern

M. Scheib – University of Kaiserslautern

Citation of published version:

Rickart, M., Mewes, T., Demokritov, S., Hillebrands, B., Scheib, M. (2004): Correlation Between Topography and Magnetic Surface Anisotropy in Epitaxial Fe Films on Vicinal-to-(001) Au Surfaces with Different Step Orientation, *Physical Review B 70*. https://doi.org/10.1103/PhysRevB.70.060408

PHYSICAL REVIEW B **70**, 060408(R) (2004)

Correlation between topography and magnetic surface anisotropy in epitaxial Fe films on vicinal-to-(001) Au surfaces with different step orientation

M. Rickart
INESC Microsistemas e Nanotecnologias, Rua Alves Redol 9, 1000 Lisboa, Portugal

T. Mewes
Department of Physics, 1077 Smith Laboratory, Ohio State University, 174 W 18th Ave, Columbus, Ohio 43210, USA

S. O. Demokritov and B. Hillebrands
Fachbereich Physik and Forschungsschwerpunkt MINAS, Technische Universität Kaiserslautern, D-67663 Kaiserslautern, Germany

M. Scheib
Institut für Oberflächen- und Schichtanalytik (IFOS) GmbH, Technische Universität Kaiserslautern, D-67663 Kaiserslautern, Germany
(Received 30 June 2004; published 31 August 2004)

For an epitaxial, vicinal surface of a magnetic film, the twofold step-induced symmetry about the film normal in the atomic coordination implies a corresponding twofold magnetic surface anisotropy. We show, that for epitaxial Fe films grown on Au surfaces vicinal to the (001) plane, tilted about the in-plane $[100]_{Au}$ or the $[110]_{Au}$ axis, a strong correlation exists between the in-plane structural anisotropy in the height-height correlation function and the magnetic surface anisotropy. This correlation is clearly evident although both anisotropies are complicated functions of the vicinal angle, the tilt axis and the film thickness due to appearing reconstructions.

DOI: 10.1103/PhysRevB.70.060408 PACS number(s): 75.30.Gw, 75.70.Rf, 68.55.−a

Understanding magnetic surface anisotropy is of paramount importance for device applications involving ultrathin magnetic films.[1] Although much progress has been made in the theoretical description in the last decade in this respect,[2–5] the surface topography in these films is often very complex, characterized by surface reconstructions and a change in roughness as a function of thickness, temperature, etc., which complicates the analysis of the resulting magnetic anisotropy. It is expected that atomic steps on the surface make a large contribution to the surface anisotropy. However, an often unavoidable distribution in the steps, both in their local density and orientation, inhibits an analytical modeling in most cases. In this communication we show that the step distribution, characterized by the height-height correlation function of the surface for different in-plane directions, may exhibit a characteristic dependence on the in-plane direction, and this structural anisotropy correlates remarkably strong with the magnetic surface anisotropy.

In a vicinal film, i.e., a film where the surface normal has a slight, but well defined, angle δ with a low-index crystallographic reference direction (so-called miscut angle or vicinal angle), steps can be well aligned. They can correspondingly make a significant contribution to magnetic surface anisotropy. Although such systems have been studied to quite some extent,[6–19] a direct correlation of the various magnetic anisotropy contributions to structural information is often outside reach.

An interesting testing ground is Fe films vicinal to (001), for which the nonvicinal case is well studied.[20–23] Growing these films on vicinal to (001) Au substrates one finds a rich variety in the surface topography. We have determined the magnetic surface anisotropy for such films with vicinal angles varying from 0.5° to 7°. The vicinal tilt axis, i.e., the axis lying in the surface plane, about which the sample was rotated out of the low-index orientation before polishing the surface, lies along either the $[100]_{Au}$ or the $[110]_{Au}$ axis.

As substrates vicinal to (001) MgO single crystals of dimensions $10\times10\times0.5$ mm^3 were used. The substrates were rinsed in isopropanol at ambient pressure before loading into a multi-chamber molecular-beam epitaxy system with a base pressure better than 5×10^{-11} mbar. The films were deposited by a five-pocket electron beam evaporator with deposition rates between 0.006 and 0.1 nm/s as monitored by a quartz microbalance. In order to remove the carbon contamination from the MgO substrates and also to smoothen the surface for improved growth of the subsequent metallic layers,[24] the substrates were treated by a low-energy atomic oxygen ion beam at room temperature prior to film deposition. Surfaces were judged clean if the Auger analysis with a sensitivity of better than 0.01 ML detected no remaining carbon contamination. Auger spectroscopy was further used to analyze the chemical composition of the samples. The analysis of the surface topography and the sample structure was performed *in situ* with low-energy electron diffraction (LEED) and reflecting high-energy electron diffraction.

To image the surface topography in real space, scanning tunneling microscopy (STM) was carried out with a commercial Park Scientific Instruments Autoprobe VP 2 UHV device. All topographic images were obtained at room temperature in a constant-current mode with a tunneling current of 0.3 nA using electrochemically etched W tips. The tip bias was 0.1 or 1 V in the case of Fe and 0.1 V for Au. Figure 1 shows some results. In order to verify the vicinal angle of the samples, x-ray diffraction using a four-circle diffractometer was performed *ex situ*.

First, a 150-nm-thick Au buffer layer was grown onto the MgO substrate using a deposition rate of 0.1 nm/s and a

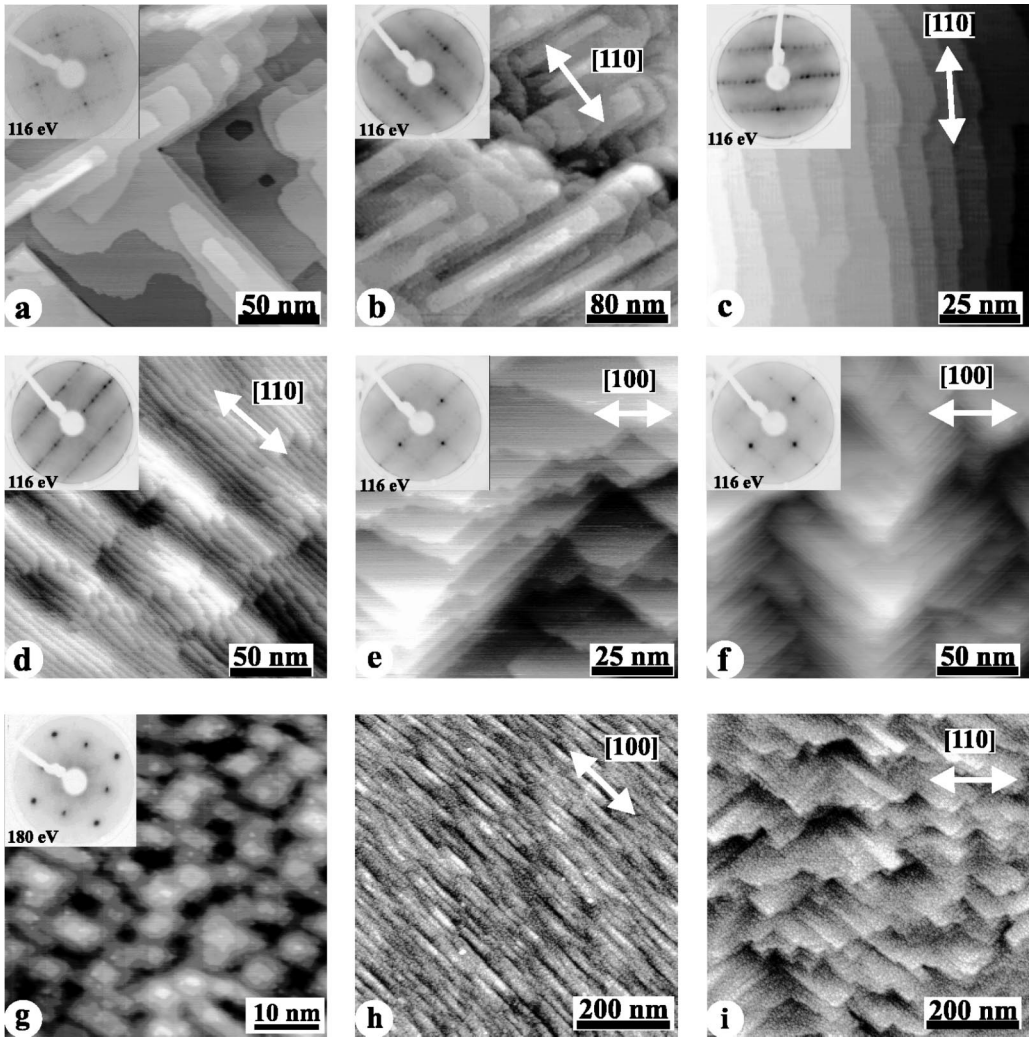

FIG. 1. STM images of the surface topography of vicinal Au(001) (a)–(f) and of vicinal Fe(001) films (g)–(i). The arrows indicate the vicinal tilt axis. (a) Au surface without miscut ($\delta=0$), the inset shows the corresponding LEED pattern with fourfold symmetry; (b) Au surface with $\delta=1°$ about the vicinal tilt axis along $[110]_{Au}$; (c) $\delta=1.5°$, $[110]_{Au}$; (d) $\delta=4°$, $[110]_{Au}$; (e) $\delta=2°$, $[100]_{Au}$; (f) $\delta=4°$, $[100]_{Au}$. (g) STM image of an Fe film showing island formation without miscut ($\delta=0$); (h) $\delta=2°$, $[100]_{Fe}$; (i) $\delta=2°$, $[110]_{Fe}$.

substrate temperature of 120 °C. Fe films were subsequently deposited at room temperature and at a rate of 0.006 nm/s. They grow in the bcc phase on fcc Au(001) with a 45° rotation of the lattice about the film normal with a corresponding in-plane lattice mismatch of less than 1%.[25,26] A small amount of 0.2 ML Au was found floating on top of the Fe surface due to an interlayer mass exchange process.[27] Fe grows quasi two-dimensional with Au acting as a self-surfactant and intermixing of the two layers can be neglected.[28] The energy dependence of the LEED spot width demonstrates an oscillating behavior, indicating that atomic steps of the Fe film roughen the surface. This is in agreement with the STM image of Fe shown in Fig. 1(g). Large islands with a mean island size of about 15 nm^2 and a height of 3–4 (ML) are observed, in agreement with previous observations.[22] The topography of the Fe films is similar to homoepitaxial growth of Fe on Fe(001) whiskers.[29] Note, that large, atomically smooth terraces and the average orientation of the step edges of the underlying Au buffers can clearly be traced on the Fe surface, as is seen in Figs. 1(h) and 1(i). The orientation of the step edges of the single Fe islands is randomly distributed.

In order to quantitatively analyze the surface topography the height-height correlation function $H(\boldsymbol{r})=\langle[z(\boldsymbol{r})-z(0)]^2\rangle$, where $z(\boldsymbol{r})$ is the surface height at position $\boldsymbol{r}$ of the surface, has been extracted using a procedure described in Ref. 30. For a self-affine and isotropic surface $H(\boldsymbol{r})$ can be expressed as

$$H(r) = 2w^2[1 - \exp(-(r/\xi)^{2\alpha})], \tag{1}$$

where α is the roughness exponent describing the texture of the roughness, ξ is the lateral correlation length defining a typical lateral size of the roughness pattern, and w is the interface width.[31] Note here that for large values of ξ, the value for α is usually low and vice versa. A typical experimental result together with a fit is demonstrated in Fig. 2. In the case of $r \ll \xi$ Eq. (1) yields $H(r) \sim r^{2\alpha}$, therefore the roughness exponent α can be easily obtained by fitting the data for $r \ll \xi$. Recently Zhao *et al.*[32] have shown that it is

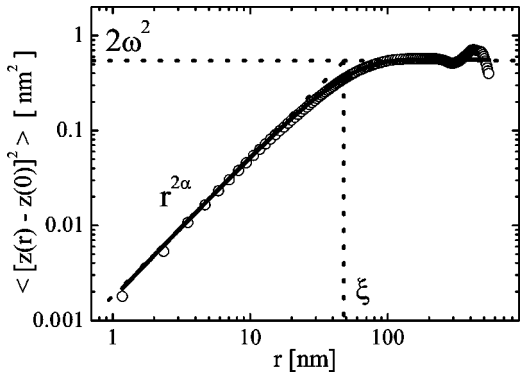

FIG. 2. Height-height correlation function extracted from the STM image of a Au film with $\delta=1°$ about the $[001]_{\mathrm{Au}}$ vicinal tilt axis. The correlation function was determined perpendicular to the tilt axis (corresponding to $\xi_\perp$, $\alpha_\perp$). The continuous line is a fit to the data (open circles).

necessary to use all three roughness parameters to describe a self-affine surface, which is the case especially for magnetic surfaces.

As the investigated surfaces are highly anisotropic, the quantification of the structural surface properties has furthermore, been extended by calculating the height-height correlation function both parallel and perpendicular to the tilt axis. Therefore two different lateral correlation lengths are used: $\xi_\perp$ and $\xi_\parallel$ for the correlation length perpendicular and parallel to the tilt axis, respectively. Analogously we use the roughness exponents $\alpha_\perp$ and $\alpha_\parallel$. From these parameters structural anisotropy parameters are derived. They are the anisotropy of the lateral correlation length Ξ, and the anisotropy of the roughness exponent $\mathcal{A}$

$$\Xi = \frac{\xi_\perp - \xi_\parallel}{\xi_\perp + \xi_\parallel} \quad \text{and} \quad \mathcal{A} = \frac{\alpha_\perp - \alpha_\parallel}{\alpha_\perp + \alpha_\parallel}. \tag{2}$$

Figure 3 shows the results obtained on the Au buffer layers. For an average orientation of the step edges, along the $[100]_{\mathrm{Au}}$ tilt axis the values of Ξ and $\mathcal{A}$ remain small over the entire range of the vicinal angle. The correlation function is nearly isotropic due to the zigzag shape of the steps [see

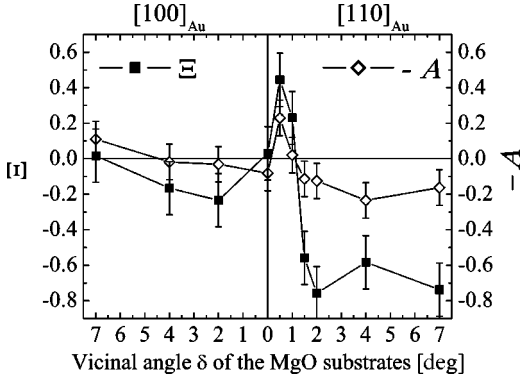

FIG. 3. Anisotropy of the lateral correlation length Ξ and anisotropy of the roughness exponent $\mathcal{A}$ of the Au surface as a function of the vicinal angle δ of the MgO substrates. In order to ease comparison with Ξ, negative values for $\mathcal{A}$ are shown.

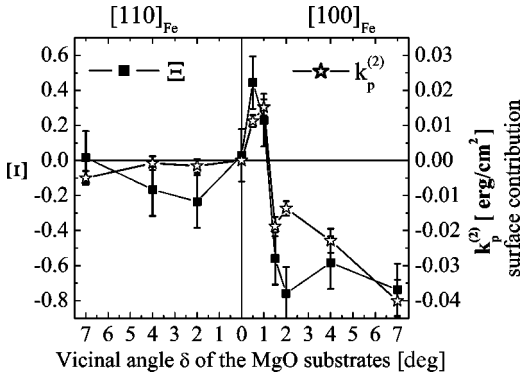

FIG. 4. Anisotropy of the correlation length Ξ of the Fe surface and surface contribution of the magnetic uniaxial in-plane anisotropy $k_p^{(2)}$ for the vicinal tilt axis along $[100]_{\mathrm{Fe}}$ (right) and $[110]_{\mathrm{Fe}}$ (left) vs the vicinal angle δ of the MgO substrates. Positive (negative) values of the anisotropy indicate an easy axis parallel (perpendicular) to the tilt axis.

Figs. 1(e) and 1(f)]. However, for the tilt axis parallel to $[110]_{\mathrm{Au}}$ a more interesting behavior is found: due to the uniaxial average orientation of the step edges the anisotropy of the correlation length, Ξ, first increases and then decreases crossing zero at an angle of about $1.3° \pm 0.2°$. This is caused by the change in topography, i.e., the change of the average orientation of the step edges with the vicinal angle as is clearly observed by STM and LEED in the images (b)–(c) in Fig. 1. In fact, for $\delta=1°$ the average orientation of the step edges is perpendicular to the tilt axis [see Fig. 1(b)]. On the other hand, it is parallel to the tilt axis for $\delta \geqslant 1.5°$ [Figs. 1(c) and 1(d)].

The magnetic anisotropies of the vicinal Fe films were derived from the frequencies of the spin waves determined by means of Brillouin light scattering spectroscopy[33,34] and the evaluation of hysteresis loops obtained by magneto-optical Kerr effect magnetometry.[11] In both cases a focused laser beam was used as a probe. The Fe films were grown in the shape of a wedge, having the advantage that a large range of Fe thicknesses (0.7–8 nm) is available on a single sample by scanning the laser beam along the wedge.

The total magnetic anisotropy energy density of a vicinal (001) film can be expressed by

$$E_{\mathrm{Ani}} = K_{s,\mathrm{eff}}^{(2)} \cdot \cos^2 \vartheta + K_{p,\mathrm{eff}}^{(4)} \cdot \sin^4 \vartheta \cdot \cos^2\varphi \cdot \sin^2 \varphi + K_{p,\mathrm{eff}}^{(2)} \cdot \sin^2\vartheta \cdot \sin^2(\varphi - \varphi_0), \tag{3}$$

where $K_{s,\mathrm{eff}}^{(2)}$, $K_{p,\mathrm{eff}}^{(2)}$, and $K_{p,\mathrm{eff}}^{(4)}$ are the effective constants of out-of-plane and in-plane uniaxial and in-plane fourfold anisotropy contributions with the attribute "effective" indicating that at this stage no separation in volume and interface contribution has been made; ϑ and φ are the polar and the azimuthal angles of the magnetization, and φ_0 (together with the sign of $K_{p,\mathrm{eff}}^{(2)}$) determines the orientation of the uniaxial in-plane easy axis with respect to the $[010]_{\mathrm{Fe}}$ axis. Thus, for $\varphi_0=0$ and $K_{p,\mathrm{eff}}^{(2)}>0$ the uniaxial easy axis coincides with $[010]_{\mathrm{Fe}}$, which is one of the easy axes of the fourfold anisotropy. Determination methods of the anisotropies can be found in Ref. 35 and references therein.

A linear dependence of the data the curve can be fitted by the usual expression $K_{p,\mathrm{eff}}^{(2)} = K_p^{(2)} + 2k_p^{(2)}/d$, where $K_p^{(2)}$ and $k_p^{(2)}$ describe the volume and surface contributions, respectively. The negative values of $K_{p,\mathrm{eff}}^{(2)}$ correspond to an easy axis of magnetization perpendicular to the average step edge orientation (perpendicular to the tilt axis) according to Eq. (3). This is the case for the samples with a miscut ranging from 1.5° to 7°.

Of central interest here is the surface contribution of the magnetic anisotropy. In Fig. 4 the surface contribution $k_p^{(2)}$ of the magnetic uniaxial in-plane anisotropy, as well as the anisotropy of the correlation length Ξ, are shown as functions of the vicinal angle for tilts about the $[100]_{\mathrm{Fe}}$ and the $[110]_{\mathrm{Fe}}$ axes. For a tilt about the $[110]_{\mathrm{Fe}}$ axis $k_p^{(2)}$ is negligibly small. This is due to the zigzag shape of the steps, which do not show any overall uniaxial step orientation. The analysis of the anisotropy in height-height correlation function of the STM images corroborates this fact. For the vicinal tilt axis along the $[100]_{\mathrm{Fe}}$ direction the anisotropy parameter Ξ of the correlation length demonstrates a change of its sign in a profound way at a vicinal angle of $\delta_c = 1.3° \pm 0.2°$ (see Fig. 1). The surface contribution of the uniaxial in-plane anisotropy $k_p^{(2)}$ and the anisotropy of the correlation length Ξ show the same behavior of their dependence on the vicinal angle. This result strongly indicates the surface nature of this effect. Thus the uniaxial surface anisotropy contribution is directly related to the structural anisotropy parameter Ξ.

To summarize we have shown that the magnetic surface anisotropy of epitaxial Fe films vicinal to (001) is strongly correlated with the surface topography of the underlying Au(001) buffer layers prepared on MgO(001) substrates. The Au buffers show a large variety in the topography dependent on the vicinal angle and the vicinal tilt axis, i.e., the $[100]_{\mathrm{Au}}$ and $[110]_{\mathrm{Au}}$ axes. The uniaxial magnetic surface anisotropy scales linearly with the structural anisotropy parameter Ξ. This result opens a new access to analyzing the influence of the surface topography on magnetic anisotropies in epitaxial thin films.

Support by the Deutsche Forschungsgemeinschaft and the European Science Foundation program NANOMAG is gratefully acknowledged.

[1] U. Gradmann, *Magnetism in Ultrathin Transition Metal Films*, in Handbook of Magnetic Materials, edited by K. H.J. Buschow (North-Holland-Elsevier, Amsterdam, 1993), Vol. 7.
[2] P. Bruno, J. Phys. F: Met. Phys. **18**, 1291 (1988).
[3] P. Bruno and J.-P. Renard, Appl. Phys. A: Solids Surf. **49**, 499 (1989).
[4] R. A. Hyman, A. Zangwill, and M. D. Stiles, Phys. Rev. B **58**, 9276 (1998).
[5] R. Arias and D. L. Mills, Phys. Rev. B **59**, 11871 (1999).
[6] B. Schulz, and K. Baberschke, Phys. Rev. B **50**, 13467 (1992).
[7] A. Berger, U. Linke, and H. P. Oepen, Phys. Rev. Lett. **68**, 839 (1992).
[8] J. Chen and J. L. Erskine, Phys. Rev. Lett. **68**, 1212 (1992).
[9] D. S. Chuang, C. A. Ballentine, and R. C. O'Handley, Phys. Rev. B **49**, 15084 (1994).
[10] R. K. Kawakami, E. J. Escorcia-Aparicio, and Z. Q. Qiu, Phys. Rev. Lett. **77**, 2570 (1996).
[11] W. Weber, R. Allenspach, and A. Bischof, Appl. Phys. Lett. **70**, 520 (1997).
[12] H. J. Choi, Z. Q. Qiu, J. Pearson, J. S. Jiang, D. Li, and S. D. Bader, Phys. Rev. B **57**, R12713 (1998).
[13] R. K. Kawakami, M. O. Bowen, H. J. Choi, E. J. Escorcia-Aparicio, and Z. Q. Qiu, Phys. Rev. B **58**, R5924 (1998).
[14] H. J. Choi, R. K. Kawakami, E. J. Escorcia-Aparicio, Z. Q. Qiu, J. Pearson, J. S. Jiang, D. Li, and S. D. Bader, Phys. Rev. Lett. **82**, 1947 (1999).
[15] T. Leeb, M. Brockmann, F. Bensch, S. Miethaner, and G. Bayreuther, J. Appl. Phys. **85**, 4964 (1999).
[16] Z. Q. Qiu and S. D. Bader, Surf. Sci. **438**, 319 (1999).
[17] H. J. Elmers, J. Hausschild, and U. Gradmann, J. Magn. Magn. Mater. **221**, 219 (2000).
[18] A. R. Frank, J. Jorzick, M. Rickart, M. Bauer, J. Fassbender, S. O. Demokritov, B. Hillebrands, M. Scheib, A. Keen, A. Petukhov, A. Kirilyuk, and Th. Rasing, J. Appl. Phys. **87**, 6092 (2000).
[19] Y. Z. Wu, C. Won, and Z. Q. Qiu, Phys. Rev. B **65**, 184419 (2002).
[20] B. Heinrich, K. B. Urquhart, A. S. Arrott, J. F. Cochran, K. Myrtle, and S. T. Purcell, Phys. Rev. Lett. **59**, 1756 (1987).
[21] Z. Q. Qiu, J. Pearson, and S. D. Bader, Phys. Rev. Lett. **70**, 1006 (1993).
[22] D. E. Bürgler, C. M. Schmidt, D. M. Schaller, F. Meisinger, R. Hofer, and H.-J. Güntherodt, Phys. Rev. B **56**, 4149 (1997).
[23] D. M. Schaller, D. E. Bürgler, C. M. Schmidt, F. Meisinger, and H.-J. Güntherodt, Phys. Rev. B **59**, 14 516 (1999).
[24] M. Rickart, B. F.P. Roos, T. Mewes, J. Jorzick, S. O. Demokritov, and B. Hillebrands, Surf. Sci. **495**, 68 (2001).
[25] P. Grünberg, S. Demokritov, A. Fuss, R. Schreiber, J. A. Wolf, and S. T. Purcell, J. Magn. Magn. Mater. **104-107**, 1734 (1995).
[26] J. J. Krebs, B. T. Jonker, and G. A. Prinz, J. Appl. Phys. **61**, 2596 (1987).
[27] O. S. Hernán, A. L. Vázquez de Parga, J. M. Gallego, and R. Miranda, Surf. Sci. **415**, 106 (1998).
[28] V. Blum, Ch. Rath, S. Müller, L. Hammer, K. Heinz, J. M. García, J. E. Ortega, J. E. Prieto, O. S. Hernán, J. M. Gallego, A. L. Vázquez de Parga, and R. Miranda, Phys. Rev. B **59**, 15 966 (1999), and references therein.
[29] J. A. Stroscio, D. T. Pierce, and R. A. Dragoset, Phys. Rev. Lett. **70**, 3615 (1993).
[30] H.-N. Yang, Y.-P. Zhao, A. Chan, T.-M. Lu, and G.- C. Wang, Phys. Rev. B **56**, 4224 (1997).
[31] S. K. Sinha, E. B. Sirota, S. Garoff, and H. B. Stanley, Phys. Rev. B **38**, 2297 (1988).
[32] Y.-P. Zhao, G. Palasantzas, G.-C. Wang, and J. Th. M. De Hosson, Phys. Rev. B **60**, 1216 (1999).
[33] S. Demokritov and E. Tsymbal, J. Phys.: Condens. Matter **6**, 7145 (1994).
[34] B. Hillebrands, in *Light Scattering in Solids*, Vol. 75 of Topics in Applied Physics, edited by H. Cardona and G. Güntherodt (Springer-Verlag, Heidelberg, 2000), p. 174.
[35] M. Rickart, S. O. Demokritov, and B. Hillebrands, J. Phys.: Condens. Matter **14**, 8947 (2002).